

# Collaboration and Competition Between Richtmyer-Meshkov instability and Rayleigh-Taylor instability

Feng Chen<sup>1\*</sup>, Aiguo Xu<sup>2,3†</sup>, Guangcai Zhang<sup>2</sup>

<sup>1</sup>*School of Aeronautics, Shan Dong Jiaotong University, Jinan 250357, China*

<sup>2</sup>*National Key Laboratory of Computational Physics,*

*Institute of Applied Physics and Computational Mathematics,*

*P.O. Box 8009-26, Beijing 100088, China*

<sup>3</sup>*Center for Applied Physics and Technology,*

*MOE Key Center for High Energy Density Physics Simulations,*

*College of Engineering, Peking University, Beijing 100871, China*

(Dated: March 1, 2022)

arXiv:1804.02642v1 [cond-mat.soft] 8 Apr 2018

---

\* Corresponding author. E-mail: shanshiwycf@163.com

† Corresponding author. E-mail: Xu\_Aiguo@iapcm.ac.cn

## Abstract

The two-dimensional Richtmyer-Meshkov Instability(RMI) system and the coexisting system combined with Rayleigh-Taylor Instability(RTI) are simulated with a multiple-relaxation time discrete Boltzmann model. It is found that, for the RMI system, the correlation between globally averaged non-organized energy flux and nonuniformity of temperature is nearly 1; the correlation between globally averaged non-organized momentum flux and nonuniformity of velocity and that between globally averaged thermodynamic non-equilibrium strength and nonuniformity of density are also high. In the coexisting system combined with RTI, the collaboration and competition mechanisms of the two instabilities are investigated. In the case where RMI dominates, an interesting interface inversion process is observed. The parameter regions for RMI dominates and RTI dominates are given. The effects of gravity acceleration and Mach number on nonequilibrium are carefully studied, via which the effects of RTI and RMI strengths on the extent of material mixing are better probed.

PACS numbers: 47.11.-j, 51.10.+y, 05.20.Dd

**Keywords:** discrete Boltzmann model/method; nonequilibrium effect; multiple-relaxation-time; Richtmyer-Meshkov instability; Rayleigh-Taylor instability

## I. INTRODUCTION

Richtmyer-Meshkov (RM)[1, 2] and Rayleigh-Taylor (RT)[3, 4] instabilities are key problems in the field of inertial confinement fusion (ICF), and also exist extensively in the fields of weapons physics, industrial processes and natural phenomena[5–7]. Therefore, the research is of important practical significance, and has attracted a wide variety of interests and got rapid development [8–22], to cite but a few.

However, in order for the problem to be tractable, most of these studies are only a separate study of RM or RT instability. Yet, RM and RT instabilities might exist simultaneously and interact with each other. For example, the uneven shape of the supernova remnant can be shown to result from the combined influence of RM and RT instabilities[23]; in the ejecta of astrophysical planetary nebulae, the internal collisions give rise to RT and RM instabilities simultaneously[24]; both RT and RM instabilities might be involved simultaneously in the deceleration phase of ICF implosions[25]; in the non-premixed combustion, both the chemically reacting RT and RM instabilities occur[26]. So, both RT and RM instabilities should be taken into account together in order to simulate the practical applications. But up to now, such studies are still relatively very little. Matsumoto et al. [27] found the synergetic growth of the RT and RM instabilities enhances the deformation of the jet interface between the relativistic jets and the surrounding medium. Meshkov and his colleagues [28] studied the features of turbulent mixing zone development at an interface accelerated by a non-stationary shock wave, and in the case of a joint effect of RT and RM instabilities emerging, the authors found that these instabilities suppress each other. He et al.[29] proposed a new hybrid-drive nonisobaric ignition scheme of ICF, and discussed the hydrodynamic instabilities during capsule implosion involving RT instability and RM instability, and they found that the linear growth rate for RT instability was significantly reduced, resulting in strong stabilization effect. Meanwhile, to our knowledge, the above research are generally based on the Euler, Navier-Stokes (NS) equations or other macroscopic continuous dynamics models, but Euler and Navier-Stokes models are not enough to describe the rich and complex nonequilibrium effects in the RT and RM system.

To overcome this constraint, we resort to the fundamental equation of non-equilibrium statistical physics, the Boltzmann equation. In principle, the Boltzmann equation works for flows in the whole range of Knudsen number (Kn). The Knudsen number is a dimensionless

number defined as the ratio of the molecular mean free path length to a representative physical length scale. From this sense, the Boltzmann works for flows with multi-scale structures, and the Knudsen number can be regarded as a measure for the continuity of flow. For a non-equilibrium flow, the Knudsen number can also be regarded as the ratio of relaxation time ( $\tau$ ) approaching local thermodynamic equilibrium to a representative time scale ( $t^R$ ) in the flow behavior. From this sense, the Knudsen number can be regarded as a kind of measure for the extent of Thermodynamic Non-Equilibrium (TNE). According to the Chapman-Enskog analysis, the Navier-Stokes equations describe just the corresponding hydrodynamic model of Boltzmann equation in the continuum limit or when the system is only slightly deviated from the local thermodynamic equilibrium. The Navier-Stokes equations are only for the evolutions of conserved kinetic moments of the distribution function (density, momentum and energy), while the Boltzmann equation describe the evolutions of all the conserved and non-conserved kinetic moments. In fact, the non-conserved kinetic moments supplement the hydrodynamic quantities in describing the specific non-equilibrium status of flow.

The Discrete Boltzmann Method (DBM) [30–32] developed from the well-known lattice Boltzmann method[33–44] aims to investigate both the Hydrodynamic and Thermodynamic Non-Equilibrium (HNE and TNE, respectively) behaviors in complex flows. It can be composed in the levels of Navier-Stokes equations[45–57], Burnett equations[32, 58–60], etc., according to the extent of TNE that the model aims to describe. It has brought some new physical insights into various complex flows[32, 60]. Besides by theory, results of DBM have been confirmed and supplemented by results of molecular dynamics[61–63], direct simulation Monte Carlo[60, 64] and experiment[56]. In the system containing both material interface and mechanical interface such as shock waves and rarefaction wave, non equilibrium characteristics can be used for the recovery of main feature of real distribution function, and provide a criterion for discriminating various interfaces, which can be used in the design of relevant interface tracking technology[50–53]. In a recent study[54], the degree of correlation between the macroscopical nonuniformity and the nonequilibrium strength in the Rayleigh-Taylor instability are systematically investigated.

Globally speaking, the research about non-equilibrium effects in the hydrodynamic instability is in its infancy. In this paper, the collaboration and competition relations between RM and RT instabilities are studied systematically, and the non-equilibrium characteristics of coupled RT and RM instabilities system are further explored.

The rest of the paper is organized as follows. Section 2 presents the MRT discrete Boltzmann model. Section 3 presents the non-equilibrium effects of RM instability system. The collaboration and competition relations between RM and RT instability are shown and analyzed in Section 4. Section 5 makes the conclusion for the present paper.

## II. DISCRETE BOLTZMANN MODEL DESCRIPTION

The MRT discrete Boltzmann equation with gravity term reads as follows

$$\frac{\partial f_i}{\partial t} + v_{i\alpha} \frac{\partial f_i}{\partial x_\alpha} = -\mathbf{M}_{il}^{-1} \hat{\mathbf{S}}_{lk} (\hat{f}_k - \hat{f}_k^{eq}) - g_\alpha \frac{(v_{i\alpha} - u_\alpha)}{RT} f_i^{eq}, \quad (1)$$

where  $f_i^{eq}$  is the equilibrium distribution function in the velocity space,  $\hat{f}_i$  and  $\hat{f}_i^{eq}$  are the particle (equilibrium) distribution functions in kinetic moment space,  $\mathbf{M}$  is the transformation matrix between the velocity space and the kinetic moment space,  $\hat{\mathbf{S}} = \text{diag}(s_1, s_2, \dots, s_N)$  is the diagonal relaxation matrix,  $g_\alpha$  is the acceleration.

The transformation matrix and the corresponding equilibrium distribution functions in kinetic moment space (KMS) can be constructed according to the seven moment relations. Specifically, the transformation matrix is  $\mathbf{M} = (m_1, m_2, \dots, m_{16})^T$ ,  $m_i = (1, v_{ix}, v_{iy}, (v_{i\alpha}^2 + \eta_i^2)/2, v_{ix}^2, v_{ix}v_{iy}, v_{iy}^2, (v_{i\beta}^2 + \eta_i^2)v_{ix}/2, (v_{i\beta}^2 + \eta_i^2)v_{iy}/2, v_{ix}^3, v_{ix}^2v_{iy}, v_{ix}v_{iy}^2, v_{iy}^3, (v_{i\chi}^2 + \eta_i^2)v_{ix}^2/2, (v_{i\chi}^2 + \eta_i^2)v_{ix}v_{iy}/2, (v_{i\chi}^2 + \eta_i^2)v_{iy}^2/2)$ . Choosing the Discrete Velocity Model (DVM) provides us with high flexibility. Here, the following discrete velocity model is adopted (see Fig. 1):

$$(v_{ix}, v_{iy}) = \begin{cases} \mathbf{cyc}: c(\pm 1, 0), & \text{for } 1 \leq i \leq 4, \\ c(\pm 1, \pm 1), & \text{for } 5 \leq i \leq 8, \\ \mathbf{cyc}: 2c(\pm 1, 0), & \text{for } 9 \leq i \leq 12, \\ 2c(\pm 1, \pm 1), & \text{for } 13 \leq i \leq 16, \end{cases} \quad (2)$$

where  $\eta_i = \eta_0$  for  $i = 1, \dots, 4$ , and  $\eta_i = 0$  for  $i = 5, \dots, 16$ . The corresponding equilibrium distribution functions in KMS are  $\hat{f}_1^{eq} = \rho$ ,  $\hat{f}_2^{eq} = j_x$ ,  $\hat{f}_3^{eq} = j_y$ ,  $\hat{f}_4^{eq} = e$ ,  $\hat{f}_5^{eq} = P + \rho u_x^2$ ,  $\hat{f}_6^{eq} = \rho u_x u_y$ ,  $\hat{f}_7^{eq} = P + \rho u_y^2$ ,  $\hat{f}_8^{eq} = (e + P)u_x$ ,  $\hat{f}_9^{eq} = (e + P)u_y$ ,  $\hat{f}_{10}^{eq} = \rho u_x(3T + u_x^2)$ ,  $\hat{f}_{11}^{eq} = \rho u_y(T + u_x^2)$ ,  $\hat{f}_{12}^{eq} = \rho u_x(T + u_y^2)$ ,  $\hat{f}_{13}^{eq} = \rho u_y(3T + u_y^2)$ ,  $\hat{f}_{14}^{eq} = (e + P)T + (e + 2P)u_x^2$ ,  $\hat{f}_{15}^{eq} = (e + 2P)u_x u_y$ , and  $\hat{f}_{16}^{eq} = (e + P)T + (e + 2P)u_y^2$ , where pressure  $P = \rho RT$  and energy  $e = b\rho RT/2 + \rho u_\alpha^2/2$ . At the continuous limit, the Navier-Stokes equations with a gravity term for both compressible and incompressible fluids can be obtained.

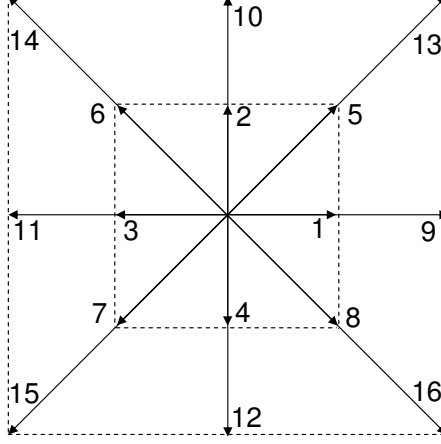


FIG. 1: Schematic of the discrete-velocity model.

The DBM inherits naturally the function of Boltzmann equation, describing nonequilibrium effects in the system. In the MRT model, the deviation from equilibrium can be defined as  $\Delta_i = \hat{f}_i - \hat{f}_i^{eq} = \mathbf{M}_{ij}(f_j - f_j^{eq})$ , and  $\Delta_i^* = \mathbf{M}_{ij}^*(f_j - f_j^{eq})$ , where  $\mathbf{M}_{ij}^*$  represent the kinetic central moments, in which the variable  $v_{i\alpha}$  is replaced by  $v_{i\alpha} - u_\alpha$ .  $\Delta_i$  contains the information of the macroscopic flow velocity, and  $\Delta_i^*$  is only the manifestation of molecular thermal motion. Corresponding to the simple definition of  $\Delta_i^*$ , some clear symbols are more commonly used, that is,  $\Delta_{2\alpha\beta}^*$ ,  $\Delta_{(3,1)\alpha}^*$ ,  $\Delta_{3\alpha\beta\gamma}^*$  and  $\Delta_{(4,2)\alpha\beta}^*$ , corresponding to  $\Delta_{5,6,7}^*$ ,  $\Delta_{8,9}^*$ ,  $\Delta_{10,11,12,13}^*$  and  $\Delta_{14,15,16}^*$ , respectively. To provide a rough estimation of Thermodynamic Non-Equilibrium (TNE), a TNE strength function  $d(x, y)$  is defined,

$$d(x, y) = \sqrt{\Delta_{2\alpha\beta}^{*2}/T^2 + \Delta_{(3,1)\alpha}^{*2}/T^3 + \Delta_{3\alpha\beta\gamma}^{*2}/T^3 + \Delta_{(4,2)\alpha\beta}^{*2}/T^4},$$

where  $d = 0$  in the thermodynamic equilibrium state and  $d > 0$  in the thermodynamic nonequilibrium state. Correspondingly, the globally averaged TNE strength  $D_{TNE}$ , Non-Organized Momentum Flux (NOMF) strength  $D_2$  and NonOrganized Energy Flux (NOEF) strength  $D_{(3,1)}$  are defined,  $D_{TNE} = \bar{d}$ ,  $D_2 = \sqrt{\Delta_{2\alpha\beta}^{*2}}$  and  $D_{(3,1)} = \sqrt{\Delta_{(3,1)\alpha}^{*2}}$ . A macroscopic nonuniformity function is also defined as

$$\delta W(x, y) = \sqrt{(W - \bar{W})^2},$$

where  $W = (\rho, U, T)$  denotes the macroscopic distribution and  $\bar{W}$  is the average value of a small cell around the point  $(x, y)$  [54].

### III. NON-EQUILIBRIUM EFFECTS OF RICHTMYER-MESHKOV INSTABILITY

The DBM model has been validated by some well-known benchmark tests, and satisfying agreements are obtained between the simulation results and analytical ones [54]. In this section, the nonequilibrium characteristics of Richtmyer-Meshkov instability system are further analyzed. Time evolution is performed through the third-order Runge-Kutta scheme, and space discretization is adopted the NND scheme.

An incident shock wave with Mach number 1.2, traveling from the top side, hits an interface with sinusoidal perturbation. The initial macroscopic quantities are as follows:

$$\left\{ \begin{array}{l} (\rho, u_1, u_2, p)_s = (3.1304, 0, -0.28005, 2.1187), \\ (\rho, u_1, u_2, p)_h = (2.3333, 0, 0, 1.4), \\ (\rho, u_1, u_2, p)_l = (1, 0, 0, 1.4), \end{array} \right.$$

where the subscripts  $s$ ,  $h$ ,  $l$  indicate the shock wave region, the heavy medium region, and the light medium region. The computational domain is a two-dimensional box with width  $W = 20.2$  and height  $H = 80$ , and divided into  $101 \times 400$  mesh-cells. Inflow boundary is applied at the top side, solid is applied at the bottom, and periodic boundary conditions are applied at the left and right boundaries.  $\gamma = 1.4$  in the whole domain.

Figure 2 shows the evolution of the fluid interface at times  $t = 0, 40, 60$ , and  $300$ . The parameters are  $c = 1$ ,  $\eta_0 = 3$ ,  $g_y = 0$ ,  $dt = 10^{-3}$ ,  $s = 10^3$ . When the shock wave passes the interface, a reflected rarefaction wave to the top and a transmission wave to the bottom are generated, and the perturbation amplitude decreases with the interface motion. Then, the peak and valley of initial interface invert, the heavy and light fluids gradually penetrate into each other as time goes on, the light fluid rises to form a bubble and the heavy fluid falls to generate a spike. The transmission wave reaches the solid wall and reflects, encounters the interface again, converts into a transmission wave penetrating into the heavy fluid zone and a reflection wave back to the light fluid. The disturbance of the interface continues to grow, eventually forming a mushroom shape.

Figure 3 shows snapshots of the TNE strength  $d$  at the same times. In the position far from the perturbation interface,  $d$  is basically 0. Around the interface,  $d$  is greater than zero. In the figure, we can find clearly the position of the material interface and the shock interface. The peak values of TNE strength  $d$  at the shock wave interface are larger than the

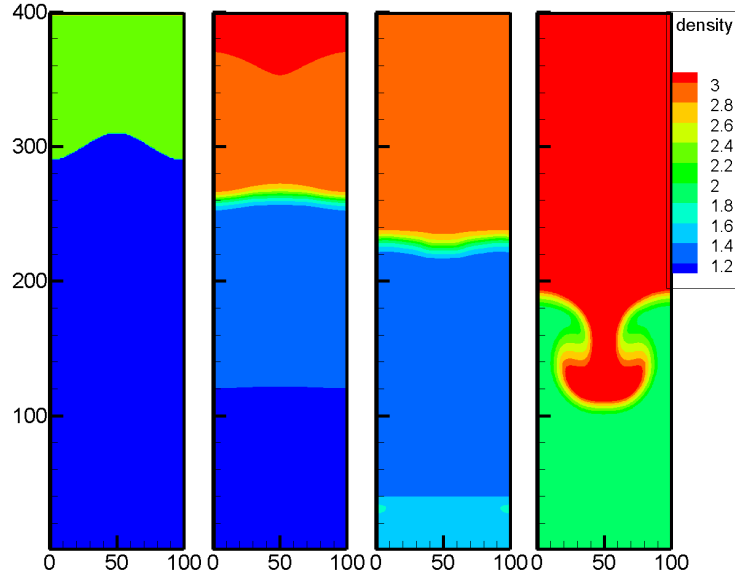


FIG. 2: Evolution of the fluid interface from a single-mode perturbation.

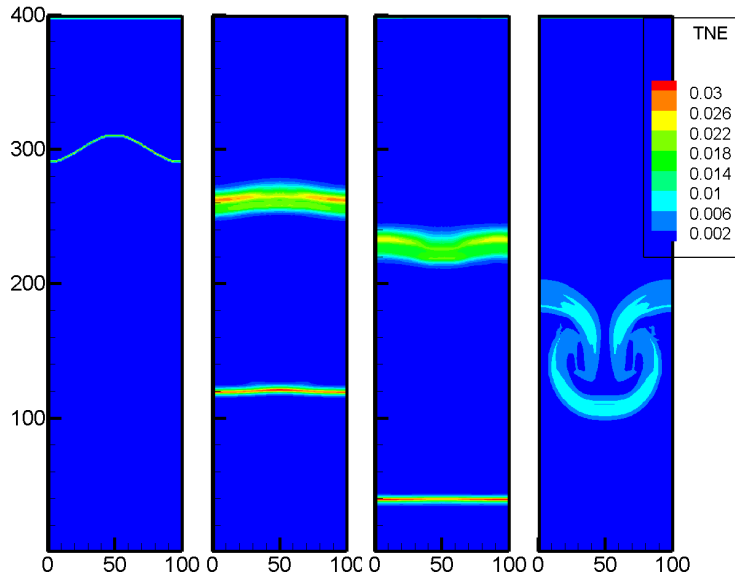


FIG. 3: Snapshots of TNE strength  $d$  at times  $t = 0, 40, 60$  and  $300$ .

material interface (and the rarefaction wave, obviously). This is because the shock dynamic procedure is faster than the other two processes, and the system has less time to relax to its thermodynamic equilibrium. This is consistent with the results in [51, 52].

Figure 4 shows the degrees of correlation between macroscopic nonuniformities and various globally averaged nonequilibrium strength values in the RM system.  $\delta\rho$ ,  $\delta T$ , and  $\delta U$  are



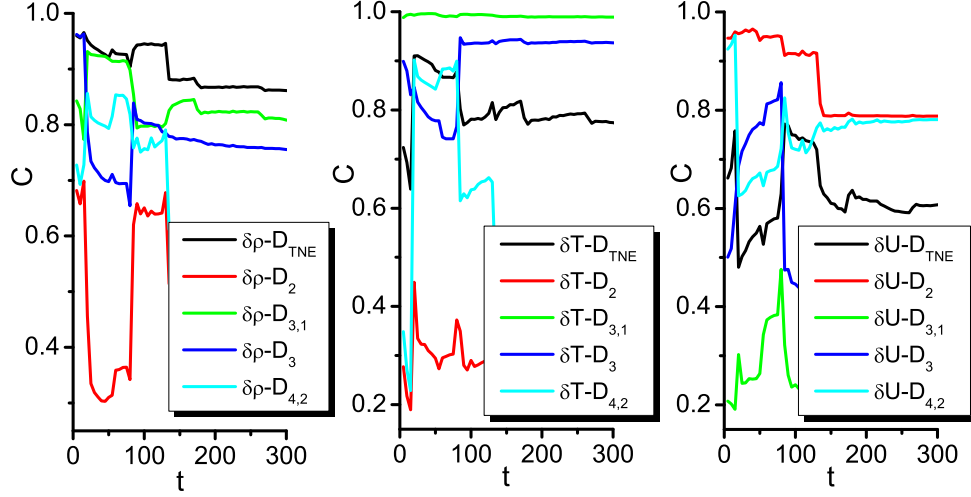


FIG. 4: Degrees of correlation between the macroscopic nonuniformities and various globally averaged nonequilibrium strength values.

density nonuniformity, temperature nonuniformity, and velocity nonuniformity, respectively. The degree of correlation between the temperature nonuniformity and the globally averaged NOEF strength  $D_{(3,1)}$  is approximately 1. The correlation between globally averaged NOMF strength and nonuniformity of velocity and that between globally averaged TNE strength and nonuniformity of density are also high.

In Figure 5, we can see that, the heat conduction plays a major role in the degrees of correlation. The greater the heat conduction, the higher the degree of correlation. Black beelines are the linear approximation of corresponding curves, that is,  $C = C_0 + k \times t$ . Choosing the proper slope  $k$ , the value of  $C_0$  will increase exponentially with the increase of heat conduction, and gradually tends to 1.

#### IV. COLLABORATION AND COMPETITION BETWEEN RM INSTABILITY AND RT INSTABILITY

In the section, the RM instability in gravitational field is simulated, and the collaboration and competition relations between RM and RT instability are studied. The initial condition

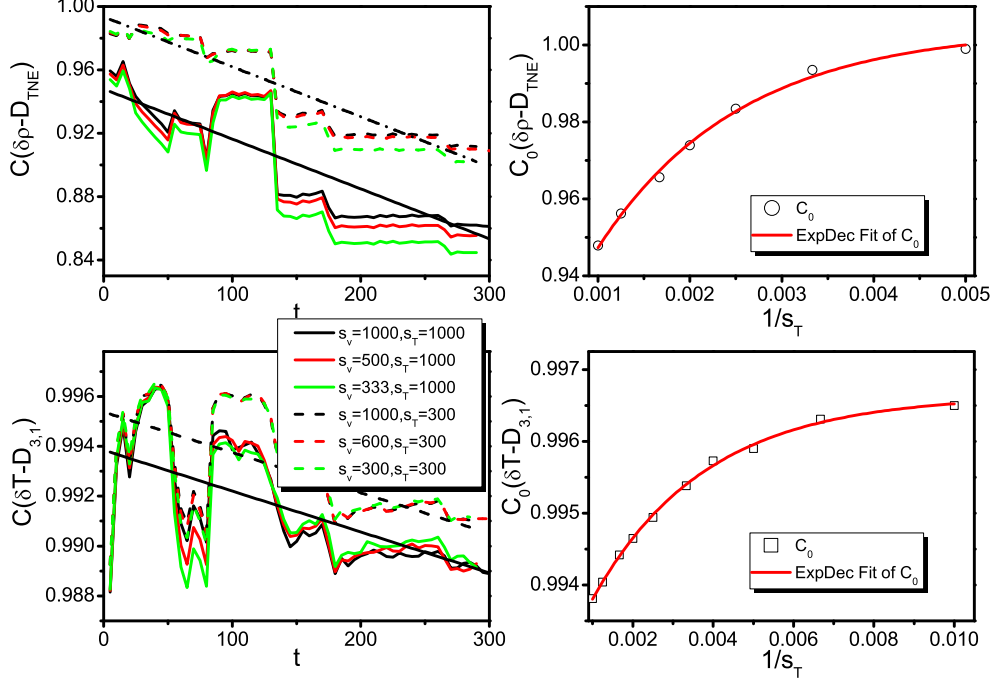


FIG. 5: Effect of heat conduction on the degree of correlation.

is replaced by the following macroscopic quantities:

$$\left\{ \begin{array}{ll} (\rho, u_1, u_2, T)_s = (3.1304 \exp(-g(y_0 - y_s)/0.6, 0, -0.28005, 0.676796), & y_0 < y \\ (\rho, u_1, u_2, T)_h = (2.3333 \exp(-g(y - y_s)/0.6, 0, 0, 0.6), & y_s < y < y_0, \\ (\rho, u_1, u_2, T)_l = (\exp(-g(y - y_s)/1.4, 0, 0, 1.4), & y < y_s, \end{array} \right.$$

where the Mach number of incident shock wave is 1.2,  $y_s$  is the initial small perturbation at the interface.

Figure 6 shows the interface amplitudes of different gravity fields. The interface inversion process is affected observably by the gravity field. There is a competition between the RM instability and RT instability, and the schematic diagram of the collaboration and competition relations are shown in Fig.7. The first line is corresponding to the case of weaker gravitational action. In the case, the RM instability plays a major role, and the interface inversion still occurs, but the inversion process is delayed. After the reversal of the interface, the gravity and shock wave jointly promote the growth of spike. The second line is the case of stronger gravitational action relative to shock wave. In the case, the RT instability plays a major role, and the interface inversion is suppressed. The light fluid rises to form a bubble and the heavy fluid falls to generate a spike. The dashed part indicates the

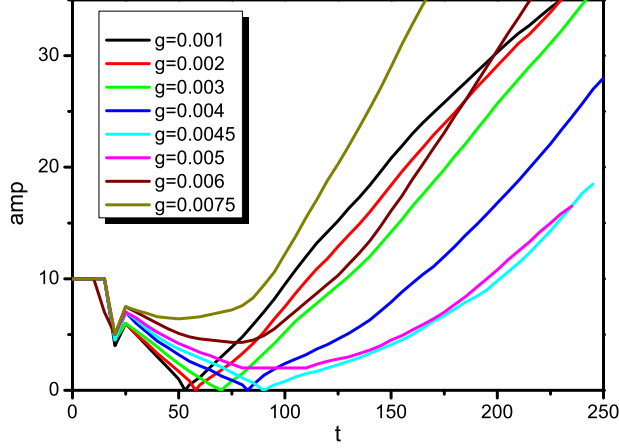


FIG. 6: Interface amplitude  $A$  in different gravity fields.

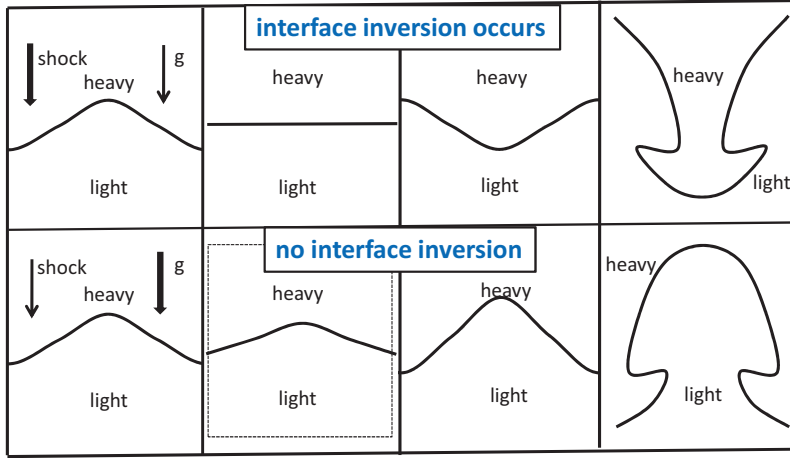


FIG. 7: The schematic diagram of the collaboration and competition relations between RM instability and RT instability.

interfacial compression process under shock wave, and the process does not occur when the impact effect is zero. The small corner at time  $t = 20$  in figure 6 indicates the process. The interface evolution of  $g = 0.002$  and  $g = 0.006$  are shown in Figure 8 and 9, respectively. We specifically explore the conditions for the interface reversal. The relationship between the Mach number and the gravitational acceleration is obtained, as shown in Figure 10. The abscissa is the Mach number, and the ordinate is the dimensionless gravitational acceleration. The trend can be expressed by a simple linear function  $g_{nond} = -0.64 + 0.59Ma$ , where  $g_{nond}$  is a dimensionless acceleration of gravity. The region below the fitting curve is the interface inversion region, i.e., RM instability plays a major role. In the region above the fitting curve,

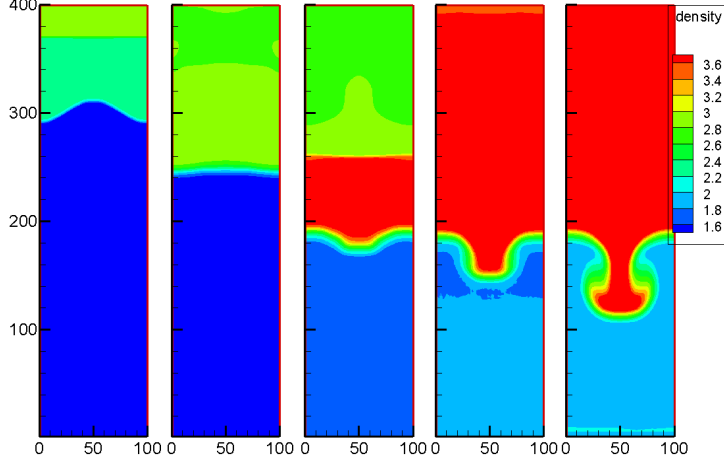


FIG. 8: The interface evolution of  $g = 0.002$  and  $Ma = 1.2$ .

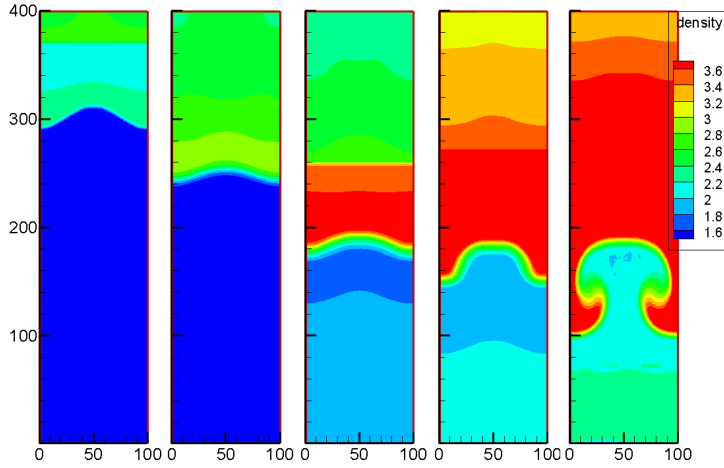


FIG. 9: The interface evolution of  $g = 0.006$  and  $Ma = 1.2$ .

the interface inversion mechanism is suppressed and RT instability plays a major role. The growth of disturbance interface near the fitting curve is suppressed farthest.

Figure 11 shows the thermodynamic nonequilibrium characteristics of the RT and RM instability coexisting system with different gravity fields. The jump at time  $t = 85$  is due to the reshock process. That is, the transmission shock wave reflects from the solid wall on the bottom and encounters the interface again. Before the reshock process, the greater the gravity  $g$ , the greater the globally averaged TNE strength  $D_{TNE}$ . This is because the larger the gravity  $g$ , the greater the density gradient. Both  $D_{TNE}$  and  $D_2$  have large attenuation at time  $t = 140$ , which is due to the reflected shock wave reaching the upper boundary. The development of  $D_{(3,1)}$  is mainly affected by the interface. During the process, the

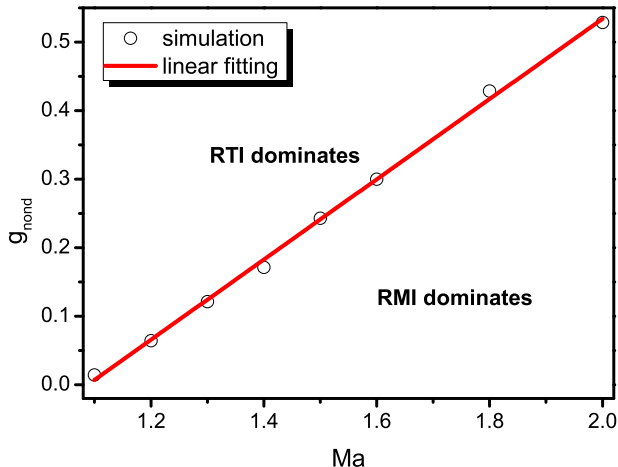


FIG. 10: The regions for interface inversion or not.

interface continues to grow, so  $D_{(3,1)}$  has no attenuation. Subsequently, for the cases where interface inversion still occurs ( $g < 0.005$ ), before the development of Kelvin-Helmholtz (KH) instability ( $t = 170$ ), the smaller the gravity, the larger the values of  $D_{TNE}$  and  $D_{(3,1)}$ . This is because the greater the gravity, the greater the resistance to inversion, making the interface smaller at this time. After the development of KH instability, the greater the gravity, the greater the growth rate of  $D_{TNE}$  and  $D_{(3,1)}$ .

In figure 12, we study the effect of Mach number on the non-equilibrium degree. Under different Mach numbers, the evolution speeds of the system are different. In order to guarantee the reliability of the analysis, the systems should have a similar degree of evolution. For convenience, we adopt the unperturbed interface, and choose the system that the transmission shock wave just reaches the solid wall as the research object. Figure (a) shows the globally averaged TNE strength with different Mach number. With the increase of Mach number, the non equilibrium degree of the system is increased. In figure (b), circles indicate the values of  $D_{TNE}$  when the shock wave with different Mach number reaches the bottom. Numerical fitting shows that the nonequilibrium degree increases exponentially with the increase of Mach number. (c) and (e) show the degrees of correlation between  $\delta\rho$  and  $D_{TNE}$ , and between  $\delta T$  and  $D_{(3,1)}$ , respectively. The dashed lines are the Origin fitting results of the corresponding real curves, and the corresponding values are represented by triangulars in (d) and squares in (f). It is shown that the degree of correlation almost exponentially decreases with the increase of Mach number.

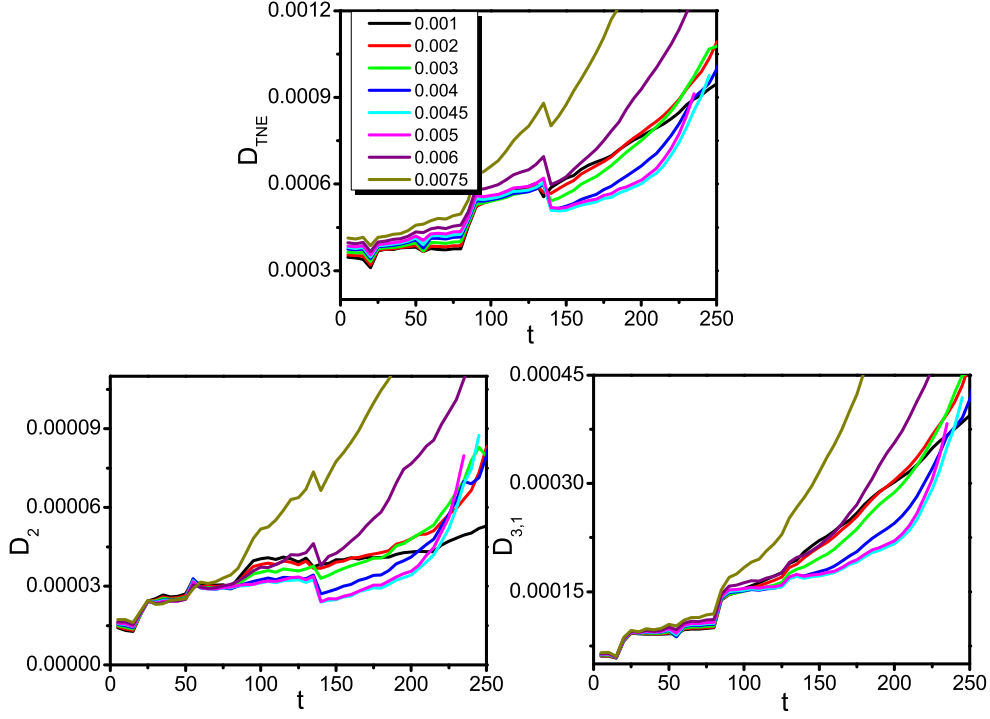


FIG. 11: The thermodynamic nonequilibrium characteristics of the RT and RM instability coexisting system with different gravity fields.

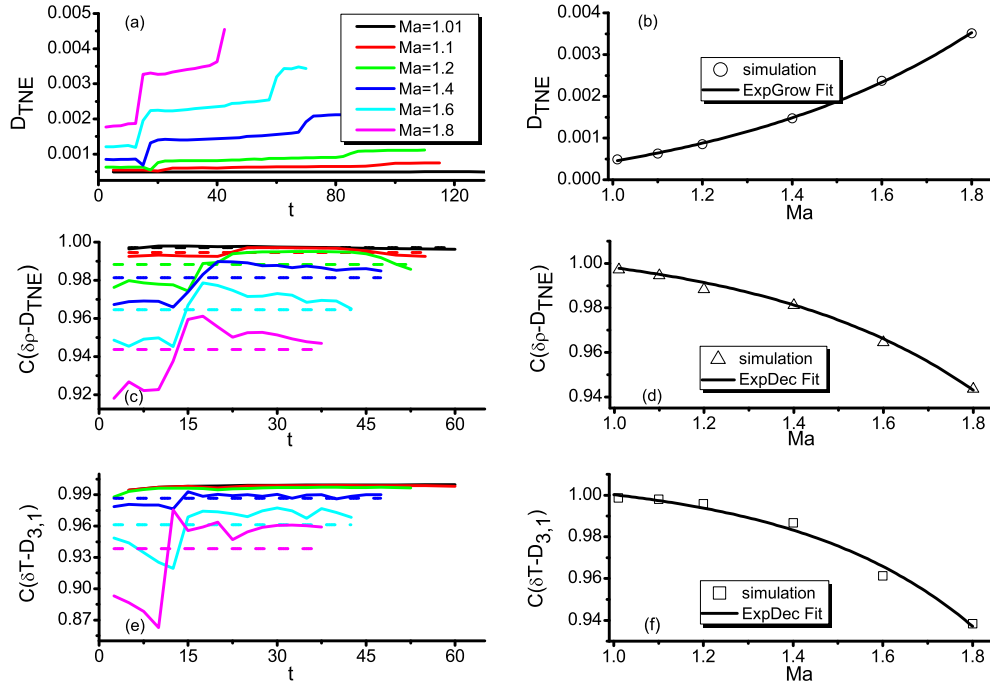


FIG. 12: Effect of Mach number on the non-equilibrium degree and the degree of correlation.

## V. CONCLUSIONS

In the paper the two-dimensional Richtmyer-Meshkov instability system and the case combined with Rayleigh-Taylor instability are simulated with a MRT discrete Boltzmann model, and the nonequilibrium characteristics are systematically investigated. The degrees of correlation between macroscopic nonuniformities and various globally averaged nonequilibrium strength values in RM instability are analyzed. Heat conduction plays a major role in the degree of correlation. The greater the heat conduction, the higher the degree of correlation. In the case combined with RT instability, the collaboration and competition mechanisms of the two instabilities are investigated, and the effects of gravity field  $g$  and Mach number on nonequilibrium are probed. (i) The interface inversion process in RM instability system is affected observably by the gravity field, and the regions for interface inversion or not are obtained. (ii) The thermodynamic nonequilibrium characteristics of the RT and RM instability coexisting system with different gravity fields get a more systematic understanding. (iii) The effect of Mach number on the non-equilibrium degree is studied. With the increase of Mach number, the non equilibrium degree of the system is increased exponentially, and the degree of correlation almost exponentially decreases with the increase of Mach number.

### Acknowledgments

We acknowledge support from the National Natural Science Foundation of China (under Grant Nos. 11402138, 11475028 and 11772064), Science Challenge Project (JCKY2016212A501), the Natural Science Foundation of Shandong Province (ZR2014EEP021) and the Foundation for Outstanding Young Scientist in Shandong Province (2012BSB01516).

- 
- [1] R. D. Richtmyer, Taylor instability in shock acceleration of compressible fluids, *Commun. Pure Appl. Maths.* 13(2), 297 (1960)
  - [2] E. E. Meshkov, Instability of the interface between of two gases accelerated by a shock wave, *Sov. Fluid Dyn.* 4(5), 101 (1969)

- [3] L. Rayleigh, Investigation of the character of the equilibrium of an incompressible heavy fluid of variable density, *Proc. London Math. Soc.* s1-14(1), 170 (1882)
- [4] G. Taylor, The Instability of Liquid Surfaces when Accelerated in a Direction Perpendicular to their Planes. I, *P. Roy. Soc. A* 201(1065), 192 (1950)
- [5] Y. Zhou, Rayleigh-Taylor and Richtmyer-Meshkov instability induced flow, turbulence, and mixing. I, *Physics Reports* 720-722, 1-136 (2017).
- [6] Y. Zhou, Rayleigh-Taylor and Richtmyer-Meshkov instability induced flow, turbulence, and mixing. II, *Physics Reports* 723-725, 1-160 (2017).
- [7] A. Xu, G. Zhang, Y. Ying, C. Wang, Complex fields in heterogeneous materials under shock: Modeling, simulation and analysis, *Sci. China: Phys. Mech. & Astron.* 59(5), 650501 (2016)
- [8] R. Betti, and J. Sanz, Bubble acceleration in the ablative Rayleigh-Taylor instability, *Phys. Rev. Lett.* 97(20), 205002 (2006)
- [9] M. R. Gupta, L. Mandal, S. Roy, and M. Khan, Effect of magnetic field on temporal development of Rayleigh-Taylor instability induced interfacial nonlinear structure, *Phys. Plasmas* 17(1), 012306 (2010)
- [10] P. K. Sharma, R. P. Prajapati, and R. K. Chhajlani, Effect of Surface Tension and Rotation on Rayleigh-Taylor Instability of Two Superposed Fluids with Suspended Particles, *Acta Phys. Pol. A* 118(4), 576 (2010)
- [11] R. Banerjee, L. K. Mandal, S. Roy, M. Khan, and M. R. Gupta, Combined effect of viscosity and vorticity on single mode Rayleigh-Taylor instability bubble growth, *Phys. Plasmas* 18(2), 022109 (2011)
- [12] G. C. Orlicz, B. J. Balakumar, C. D. Tomkins, K. P. Prestridge, A Mach number study of the Richtmyer-Meshkov instability in a varicose, heavy-gas curtain, *Phys. Fluids* 21(6), 064102 (2009)
- [13] W. Mostert, V. Wheatley, R. Samtaney, and D. I. Pullin, Effects of magnetic fields on magnetohydrodynamic cylindrical and spherical Richtmyer-Meshkov instability, *Phys. Fluids* 27(10), 104102 (2015)
- [14] K. O. Mikaelian, Rayleigh-Taylor and Richtmyer-Meshkov instabilities and mixing in stratified cylindrical shells, *Phys. Fluids* 17(9), 094105 (2005)
- [15] M. Latini, O. Schilling, and W. S. Don, High-resolution simulations and modeling of reshocked single-mode Richtmyer-Meshkov instability: Comparison to experimental data and to ampli-



- tude growth model predictions, *Phys. Fluids* 19(2), 024104 (2007)
- [16] B. L. Tian, D. X. Fu and Y. W. Ma, Numerical investigation of Richtmyer- Meshkov instability driven by cylindrical shocks, *Acta Mech. Sinica* 22(1), 9 (2006)
- [17] F. J. Gao, Y. S. Zhang, Z. W. He, B. L. Tian, Formula for growth rate of mixing width applied to Richtmyer-Meshkov instability, *Phys. Fluids* 28(11), 114101 (2016)
- [18] F. Chen, A. Xu , G. Zhang , Y. Li , Multiple-Relaxation-Time Lattice Boltzmann Approach to Richtmyer-Meshkov Instability, *Commun. Theor. Phys.* 55(2) 325 (2011)
- [19] L. Biferale, F. Mantovani, M. Sbragaglia, A. Scagliarini, F. Toschi, R. Tripiccione, Reactive Rayleigh-Taylor systems: Front propagation and non-stationarity, *Europhys. Lett.* 94(5), 54004 (2011)
- [20] G. J. Liu, Z. L. Guo, Effects of Prandtl number on mixing process in miscible Rayleigh-Taylor instability: A lattice Boltzmann study, *Int. J. Numer. Method. H.* 23(1), 176 (2013)
- [21] L. F. Wang, W. H. Ye, J. F. Wu, Jie Liu, W. Y. Zhang, X. T. He, A scheme for reducing deceleration-phase Rayleigh-Taylor growth in inertial confinement fusion implosions, *Phys. Plasmas* 23(5), 052713 (2016)
- [22] I. Maimouni, J. Goyon, E. Lac, T. Pringuey, J. Boujlel, X. Chateau, P. Coussot, Rayleigh-Taylor Instability in Elastoplastic Solids: A Local Catastrophic Process, *Phys. Rev. Lett.* 116(15), 154502 (2016)
- [23] B. Aschenbach, R. Egger, J. Tromper, Discovery of explosion fragments outside the Vela supernova remnant shock-wave boundary, *Nature* 373, 587 (1995)
- [24] B. Balick and A. Frank, Shapes and Shaping of Planetary Nebulae, *Annual Review of Astronomy and Astrophysics*, 40, 439 (2002)
- [25] P. A. Bradley, The effect of mix on capsule yields as a function of shell thickness and gas fill, *Phys. Plasma* 21(6), 062703 (2014)
- [26] N. Attal and P. Ramaprabhu, Numerical investigation of a single-mode chemically reacting Richtmyer-Meshkov instability, *Shock Waves* 25(4), 307 (2015)
- [27] J. Matsumoto and Y. Masada, Two-dimensional numerical study for Rayleigh-Taylor and Richtmyer-Meshkov instabilities in relativistic jets, *Astrophys. J. Lett.* 772, 1 (2013)
- [28] E. E Meshkov, Some peculiar features of hydrodynamic instability development, *Phil Trans. R. Soc. A* 371(2003), 20120288 (2013)
- [29] X. T. He, J. W. Li, Z. F. Fan, L. F. Wang, J. Liu, K. Lan, J. F. Wu, A hybrid-drive nonisobaric-

- ignition scheme for inertial confinement fusion, *Phys. Plasmas* 23(8), 082706 (2016)
- [30] A. Xu, G. Zhang, Y. Ying, Progress of discrete Boltzmann modeling and simulation of combustion system, *Acta Phys. Sin.* 64(18), 184701 (2015)
- [31] A. Xu, G. Zhang, Y. Gan, Progress in studies on discrete Boltzmann modeling of phase separation process, *Mech. Eng.* 38(4), 361 (2016)
- [32] A. Xu, G. Zhang and Y. Zhang, Discrete Boltzmann Modeling of Compressible Flows, Chapter 2 in *Kinetic Theory* edited by G. Z. Kyzas and A. C. Mitropoulos, Rijeka: InTech, 2018.
- [33] S. Succi, *The Lattice Boltzmann Equation for Fluid Dynamics and Beyond*, Oxford: Oxford University Press, 2001
- [34] R. Benzi, S. Succi, and M. Vergassola, The lattice Boltzmann equation: Theory and applications, *Phys. Rep.* 222(3), 145 (1992)
- [35] A. Xu, G. Zhang, Y. Gan, F. Chen, X. Yu, Lattice Boltzmann modeling and simulation of compressible flows, *Front. Phys.* 7(5), 582 (2012)
- [36] W. R. Osborn, E. Orlandini, M. R. Swift, J. M. Yeomans, J. R. Banavar, Lattice boltzmann study of hydrodynamic spinodal decomposition, *Phys. Rev. Lett.* 75(22), 4031 (1995).
- [37] H. Li, X. Lu, H. Fang, Y. Qian, Force evaluations in lattice boltzmann simulations with moving boundaries in two dimensions, *Phys. Rev. E* 70(2), 026701 (2004).
- [38] Y. Zhang, R. Qin, and D. Emerson, Lattice Boltzmann simulation of rarefied gas flows in microchannels, *Phys. Rev. E* 71(4), 047702 (2005)
- [39] X. Shan, X. Yuan and H. Chen, Kinetic theory representation of hydrodynamics: a way beyond the Navier-Stokes equation, *J Fluid Mech.* 550, 413 (2006)
- [40] Y. Wang, C. Shu, H. Huang, et al. Multiphase lattice Boltzmann flux solver for incompressible multiphase flows with large density ratio. *J Comput. Phys.* 280, 404 (2015)
- [41] K. Qu, C. Shu and Y. Chew, Alternative method to construct equilibrium distribution functions in lattice-Boltzmann method simulation of inviscid compressible flows at high Mach number. *Phys. Rev. E* 75, 036706 (2007)
- [42] C. Zhuo, C. Zhong and J. Gao, Filter-matrix lattice Boltzmann model for incompressible thermal flows, *Phys. Rev. E* 85,046703 (2012)
- [43] K. Li, C. Zhong, A lattice Boltzmann model for simulation of compressible flows, *Int. J. Numer. Meth. Fluids* 77(6),334 (2015)
- [44] Y. Zhang, R. Qin, Y. Sun, R. W. Barber, and D. R. Emerson, Gas flow in microchannels

- lattice Boltzmann method approach, *J. Stat. Phys.* 121(11C2), 257 (2005).
- [45] B. Yan, A. Xu, G. Zhang, Y. Ying, H. Li, Lattice Boltzmann model for combustion and detonation, *Front. Phys.* 8(1), 94 (2013)
- [46] Y. Gan, A. Xu, G. Zhang, S. Succi, Discrete Boltzmann modeling of multiphase flows: hydrodynamic and thermodynamic non-equilibrium effects, *Soft Matter* 11(26), 5336 (2015)
- [47] A. Xu, C. Lin, G. Zhang, Y. Li, Multiple-relaxation-time lattice Boltzmann kinetic model for combustion, *Phys. Rev. E* 91(4), 043306 (2015)
- [48] C. Lin, A. Xu, G. Zhang, Y. Li, Double-distribution-function discrete Boltzmann model for combustion, *Combust. Flame* 164,137(2016)
- [49] Y. Zhang, A. Xu, G. Zhang, C. Zhu, and C. Lin, Kinetic modeling of detonation and effects of negative temperature coefficient, *Combust. Flame* 173, 483 (2016)
- [50] C. Lin, A. Xu, G. Zhang, K. Luo, Y. Li, Discrete Boltzmann modeling of Rayleigh-Taylor instability in two-component compressible flows, *Phys. Rev. E* 96, 053305 (2017)
- [51] C. Lin, A. Xu, G. Zhang, Y. Li, S. Succi, Polar-coordinate lattice Boltzmann modeling of compressible flows, *Phys. Rev. E* 89(1), 013307 (2014)
- [52] F. Chen, A. Xu, G. Zhang, Y. Wang, Two-dimensional MRT LB model for compressible and incompressible flows, *Front. Phys.* 9(2), 246 (2014)
- [53] H. Lai, A. Xu, G. Zhang, Y. Gan, Y. Ying, S. Succi, Non-equilibrium thermohydrodynamic effects on the Rayleigh-Taylor instability incompressible flow, *Phys. Rev. E* 94(2), 023106 (2016)
- [54] F. Chen, A. Xu, and G. Zhang, Viscosity, heat conductivity, and Prandtl number effects in the Rayleigh-Taylor Instability, *Front. Phys.* 11(6), 114703 (2016)
- [55] C. Lin, K. Luo, MRT discrete Boltzmann method for compressible exothermic reactive flows, *Computers and Fluids* 166, 176 (2018).
- [56] C. Lin, K. Luo, L. Fei, S. Succi, A multi-component discrete Boltzmann model for nonequilibrium reactive flows, *Sci. Rep.* 7, 14580 (2017).
- [57] A. Xu, G. Zhang, Y. Zhang, P. Wang, Y. Ying, Discrete Boltzmann model for implosion and explosion related compressible flow with spherical symmetry, *Front. Phys.*(2018,in press); arXiv:1803.03117.
- [58] Y. Zhang, A. Xu, G. Zhang, Z. Chen, P. Wang, Discrete ellipsoidal statistical BGK model and Burnett equations, *Front. Phys.* 13(3), 135101 (2018).

- [59] Y. Gan, A. Xu, G. Zhang, Y. Zhang, S. Succi, Discrete Boltzmann trans-scale modeling of high-speed compressible flows, arXiv:1801.04522
- [60] Y. Zhang, A. Xu, G. Zhang, Z. Chen, P. Wang, Discrete Boltzmann method for nonequilibrium flows: based on Shakhov model, (Submitted to J. Fluid Mech.)
- [61] H. Liu, W. Kang, Q. Zhang, Y. Zhang, H. Duan, and X. T. He, Molecular dynamics simulations of microscopic structure of ultra strong shock waves in dense helium, *Front. Phys.* 11(6), 115206 (2016)
- [62] H. Liu, Y. Zhang, W. Kang, P. Zhang, H.L. Duan and X.T. He, Molecular dynamics simulation of strong shock waves propagating in dense deuterium, taking into consideration effects of excited electrons. *Phys. Rev. E* 95(7), 023201 (2017)
- [63] H. Liu, W. Kang, H. Duan, P. Zhang, X. He, Recent progresses on numerical investigations of microscopic structure of strong shock waves in fluid, *Scientia Sinica Physica Mechanica & Astronomica* 47(7), 070003, 2017.
- [64] J. Meng, Y. Zhang, N. G. Hadjiconstantinou, G. A. Radtke, and X. Shan, Lattice ellipsoidal statistical BGK model for thermal non-equilibrium flows, *J. Fluid Mech.* 718, 347 (2013)